PRAMANA
— journal of
physics

Vol. 71, No. 4
October 2008
pp. 729–738

Polymer dynamics from synthetic polymers to proteins

D RICHTER[1,*], R BIEHL[1], M MONKENBUSCH[1], B HOFFMANN[2] and R MERKEL[2]
[1]Institut für Festkörperforschung, [2]Institut für Bio- und Nanosysteme, Forschungszentrum Jülich, D-52425 Jülich, Germany
*Corresponding author. E-mail: d.richter@fz-juelich.de

Abstract. Starting from the standard model of polymer motion – the Rouse model – we briefly present some key experimental results on the mesoscopic dynamics of polymer systems. We touch the role of topological confinement as expressed in the reptation model and discuss in some more detail processes limiting the confinement. In the second part we relate to some new developments concerning the measurement of large-scale internal dynamics of proteins by neutron spin echo.

Keywords. Polymer dynamics; reptation; domain dynamics biomolecules.

PACS Nos 87.15.H; 87.14.E; 87.64.Bx; 83.80.Sg; 61.12.Ex

The drive towards the molecular understanding of the complex viscoelastic properties of polymer liquids is the focal point of rheology and connects the classical chemical engineering approach with modern physics [1]. There, the tube model invented by Doi and Edwards [2] and de Gennes [3] has shown itself as the most successful molecular model describing the topological confinement imposed by the mutually interpenetrating polymer chains in the melt. In terms of this reptation model, a theory of viscoelasticity has been developed that describes the main features of polymer melt rheology.

Large-scale protein motions on the other hand are critical for proteins to coordinate precise biological functions. Structural studies have documented the conformational flexibility in proteins accompanying their activity. Results from macroscopic studies such as biochemical kinetics and single molecule detections have also shown the importance of conformational dynamics and Brownian thermal fluctuations within proteins or protein complexes. However, the time-dependent dynamic processes that facilitate such protein motions remain poorly understood and experimentally nearly untouched [4].

Neutron spin echo spectroscopy provides time resolution in the 100 ns range enabling thereby the access to molecular motion on a mesoscopic time scale between the atomic picosecond scales and the macroscopic times [5]. At that scale the molecular motions of the polymers take place that underlie their macroscopic

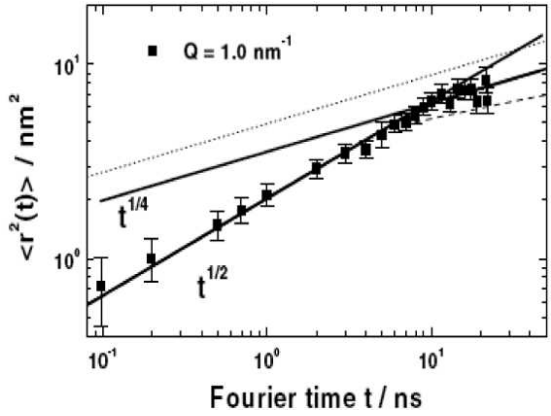

Figure 1. Time-dependent mean square displacement of a PEP segment in the melt at 492 K. The solid line indicates the prediction of the Rouse model [6]. The slowing down at longer times is an indication of a cross-over to local repation (see ref. [6]).

viscoelastic behaviour. The large-scale motions of biomolecules occur on similar space time frames [6–13].

We start with the 'standard model' for the dynamics of a polymer chain in a dense environment, the so-called Rouse model. This model treats the dynamics of a Gaussian chain in a heat bath, thereby only entropic forces originating from the conformational chain entropy and random thermal forces are considered. At scales $Q \cdot R_{\mathrm{E}} > 1$ where R_{E} is the chain end to end distance, in Gaussian approximation the self-correlation function for this model assumes a simple form [14].

$$S_{\mathrm{self}}(Q,t) = \exp\left[-\frac{Q^2}{6}\langle r^2(t)\rangle\right] = \exp\left[-\frac{Q^2}{3}\left(\frac{W\ell^4}{\pi}t\right)^{1/2}\right], \tag{1}$$

where

$$\langle r^2(t)\rangle = \frac{1}{2}\left(\frac{W\ell^4}{\pi}t\right)^{1/2}.$$

The first part displays the general form of the Gaussian approximation showing that a measurement of the self-correlation function yields direct access to the mean square displacement of a diffusing particle. The second part presents the specific prediction of the Rouse model. Thereby, $W = 3k_{\mathrm{B}}T/(\zeta\ell^2)$ is the elementary Rouse frequency. It is given by the ratio of the entropic force $3k_{\mathrm{B}}T/\ell^2$ and the friction coefficient $\zeta \cdot \ell^2$ is the mean square segment length. Note that the Rouse model predicts an anomalous sublinear segment diffusion in time.

Figure 1 presents a measurement of the segment mean square displacement on a fully protonated melt of polyethylene propylene of molecular weight $M_{\mathrm{w}} = 80{,}000$ g/mol [6]. It is evident that the mean square displacement follows the predicted $t^{1/2}$ behaviour very well for two orders of magnitude in time.

For long chains topological chain/chain interactions in terms of entanglements become important and dominate the dynamical behaviour. In the reptation model these constraints are described by a virtual tube which localizes a given chain and limits its motion to a 1d Rouse motion inside the tube (local reptation) and a slow diffusive creep motion out of the tube (reptation) [14]. Applying NSE spectroscopy it has become possible to observe the dynamic structure factor $S(Q,t)$ associated with tube confinement and local reptation. de Gennes [3] and Doi and Edwards [2] have formulated a tractable analytic expression for the dynamic structure factor which is composed of two contributions, $S^{\mathrm{loc}}(Q,t)$ and $S^{\mathrm{esc}}(Q,t)$ reflecting local reptation and the escape processes (creep motion) from the tube.

$$\frac{S_{\mathrm{chain}}(Q,t)}{S_{\mathrm{chain}}(Q)} = \left[1-\exp\left(-\frac{Q^2d^2}{36}\right)\right] S^{\mathrm{loc}}(Q,t) + \exp\left(-\frac{Q^2d^2}{36}\right) S^{\mathrm{esc}}(Q,t). \tag{2}$$

The local reptation part was calculated as [15]

$$S^{\mathrm{loc}}(Q,t) = \exp\left(\frac{t}{\tau_0}\right) \mathrm{erfc}\left[\left(\frac{t}{\tau_0}\right)^{1/2}\right], \tag{3}$$

where $\tau_0 = 36/(W\ell^4Q^4)$ and d is the tube diameter. For long chains at short time S_{chain} decays mainly through local reptation while for longer times the second term describing the creep dominates. The ratio of the two relevant time scales τ_0 and τ_{d} (disentanglement time) is proportional to N^3 (N: number of monomers along the chain). Therefore, at intermediate times $\tau_{\mathrm{E}} < t < \tau_{\mathrm{d}}$ a pronounced plateau in $S_{\mathrm{chain}}(Q,t)$ is predicted. Such a plateau is a signature for a confined motion.

Figure 2 displays the dynamic structure factor from a long chain polyethylene (PE) melt showing very clearly the tendency to form a plateau at high time [8]. In the spirit of eq. (2) and neglecting the ongoing decay of $S_{\mathrm{chain}}(Q,t)$ due to local reptation, from the plateau heights we may obtain a first estimate for the size of the confinement. Identifying the plateau levels with a Debye–Waller factor, a confinement length of $d = 45$ Å is obtained while a full evaluation results in a tube diameter of $d = 48$ Å. We note that at present the de Gennes dynamic structure factor is the only analytical model so far published which is able to describe the dynamic structure factor data.

It is well-known that a number of salient properties of entangled polymer melts are only qualitatively in agreement with reptation, indicating the existence of additional processes that release topological confinement [9]. These processes comprise fluctuating chain ends which open a route to escape the tube confinement (contour length fluctuations, CLF) and the lateral tube opening by diffusion processes of confining chains (constraint release, CR). Both mechanisms are depicted schematically in figure 3. Here we concentrate on CLF which is an effect of the confined chain itself.

CLF originate from the fluctuations of the primitive path length of the tube and are key mechanisms for the relaxation at earlier times and are also the basis for hierarchical relaxation processes of branched polymers where CLF are considered

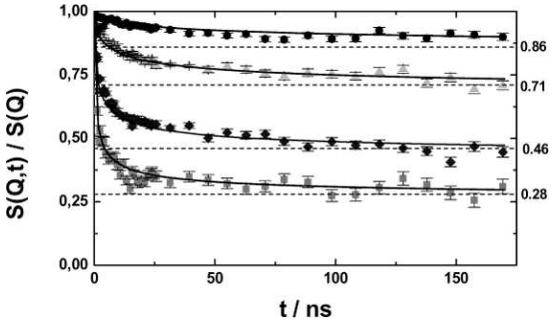

Figure 2. The dynamic structure factor from a $M_w = 36$ kg mol^{-1} PE melt at 509 K as a function of time. The solid lines are a fit with the reptation model (eq. (2)). The Q values from the top are $Q = 0.5$, 0.77, 1.15 and 1.45 nm^{-1}. The horizontal dashed lines display the prediction of the Debye–Waller factor estimate for the confinement size (see text).

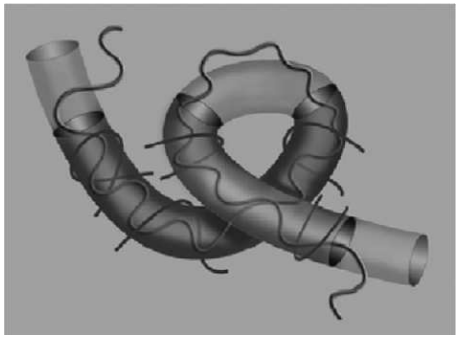

Figure 3. Schematic presentation of the CLF and CR mechanisms: chain end fluctuations lead to a shortening of the effective tube length, while the dissolving of entanglements allow chain motions beyond the initial tube constraints [12].

to be the fundamental process facilitating the release of side branches. Any chain retraction and subsequent expansion lead to a loss of memory of the original confining tube. Thus, effectively the tube becomes shorter with time. Mathematically the problem may be treated as a first passage problem. Whenever a tube contour is visited by the free end it ceases to exist. The functional form of the tube survival probability $\mu(t)$ was derived from scaling arguments [16].

$$\mu(t) = 1 - \frac{C_\mu}{Z}\left(\frac{t}{\tau_e}\right)^{1/4}. \tag{4}$$

The constant $C_\mu = 1.5 \pm 0.02$ was obtained from stochastic simulations. $Z = N/N_e$ is the number of entanglements, N_e is the number of segments forming an entanglement strand and τ_e is the relaxation time of an entanglement strand. Equation (4) describes quantitatively which chain fraction at a time t is still confined. All

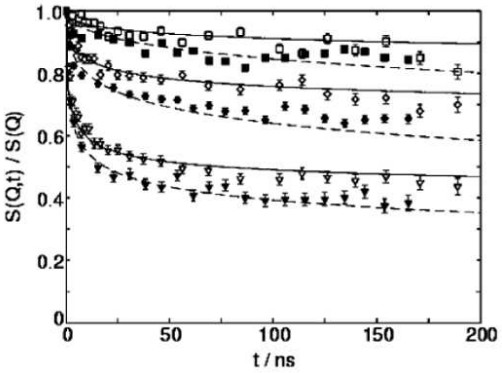

Figure 4. Dynamic structure factor of a centre-labelled 25 kg mol^{-1} PE chain (filled symbols) compared to a fully labelled chain (open symbols) of the same overall molecular weight. Q values (in nm^{-1}): 0.5 (squares), 0.77 (diamonds), 0.96 (circles), 1.15 (triangles). Lines: for centre-labelled chain, pure reptation model (eq. (2)); for fully labelled 25 kg mol^{-1} chain (dashed) CLF was considered [11,17].

parameters are known from the NSE experiments on the dynamics of asymptotically long chains (see above) where the CLF effect does not play any role.

With this knowledge, eq. (4) allows the design of an experiment where the CLF effect may be directly demonstrated [11]. In this experiment the dynamic structure factor of a fully labelled chain is compared with that of an identical chain where the contrast of those segments which are affected by CLF within the experimental time frame was matched. In such a case the dynamics should be equal to those of an asymptotically long fully confined chain.

With the known parameters for PE, eq. (4) gives that at 509 K, the experimental temperature, on average on each side 220 monomers are released during an observation time of 190 ns. The above-described experiments were performed on two different PE chains of a molecular weight of 25 kg mol^{-1} one of which was fully hydrogenated and the other having deuterated labels of $M_{\mathrm{w}} = 4$ kg mol^{-1} corresponding to 260 monomers on each end. Both were studied in a deuterated matrix of the same molecular weight.

Figure 4 presents the normalized dynamic structure factor $S(Q,t)/S(Q)$ for different Q values for the two chains. In all cases at short times the structure factor displays a strong initial decay which is due to the initial free Rouse motion. For longer times the decay is strongly reduced, transgressing into the confinement-related plateau behaviour. Comparing the levels of decay, we realize that the structure factor from the fully labelled chain decays significantly stronger than that from the corresponding centre labelled counterpart.

Apparently the constraints for the centre-labelled chain are stronger than those for the chain where the ends are visible. We further note that in the case where the ends were masked the centre part of the chain shows exactly the same structure factor as that from a very long chain, signifying directly the action of CLF at the chain ends and the remaining full confinement of the centre.

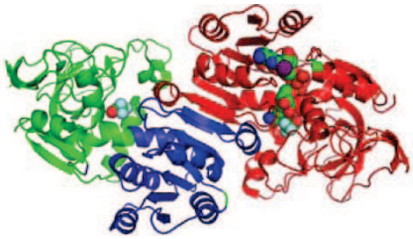

Figure 5. Dimer of alcohol dehydrogenase. The molecule presented by spherical caps is the NAD cofactor used in the chemical reaction.

Concluding this paragraph we may emphasize that neutron spin echo spectroscopy in combination with synthetic chemistry is able to unravel the important dynamical mechanisms ruling the complex chain dynamics in polymer melts on a molecular scale. We have demonstrated the astonishing validity of the Rouse model in its space time frame. We then have shown the molecular existence of the tube confinement in long chain polymer melts, thereafter we have alluded to mechanisms inherent to the tube model which limit the confinement. Using sophisticated anionic polymerization chemistry the CLF mechanism which dismantles the tube from its end was unambiguously demonstrated laying also the molecular foundation for the basic process in the hierarchical relaxation of branched polymers.

With the study of polymer dynamics reaching some maturity, the next challenge will be to unravel the large-scale motion of biopolymers and to find out to what extent these dynamics play a role in their function. While at present the conformational dynamics on local scales have been successfully approached by e.g. time-dependent crystallography [18], large-scale dynamics such as protein domain motions remain basically untouched experimentally, because of the lack of techniques to study these large-scale correlated motions. Here we present some first results on the domain dynamics of alcohol dehydrogenase (ADH). The alcohol dehydrogenases are enzymes that are present in many organisms, allowing the interconversion between alcohols and ketones. In humans it catalyses the oxidation of ethanol and is always present in the form of a dimer. In yeast it is at the basis of the fermentation process and converts acetaldehyde into ethanol. In the process the cofactor NAD is needed in assisting the oxidation reaction.

Figure 5 displays a schematic structure of a dimer based on crystallographic data. The figure displays the dimer with the two monomeric units clearly visible. Each monomer is build from two domains with a small opening in between where the cofactor NAD is placed which assists the oxidation process at the zinc active site. Some of the questions to answer are to what extent the domain dynamics assists the incorporation of the cofactor into the narrow slit between the cofactor binding and the catalytic domain and whether the cofactor itself may modify the domain dynamics.

In our studies we used ADH from yeast which forms a tetramer structure. The crystallographic data show a crossed arrangement of the two dimers. In order to verify whether in solution a similar tetrameric aggregate is present, neutron small angle scattering experiments were performed as a function of concentration. Figure 6 presents the SANS data together with a comparison with a number of models

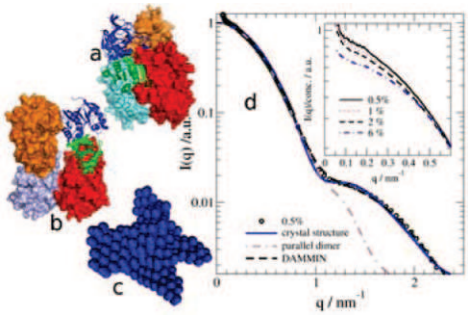

Figure 6. SANS results on ADH solutions of different concentrations (**d**). Insert: concentration-dependent results. The different curves in the main figure display modelling results for various dimer arrangements. (**a**) Solid line: crystal structure; (**b**) thin solid line: DAMMIN result, (**c**) dashed–dotted line: planar dimers at close contact.

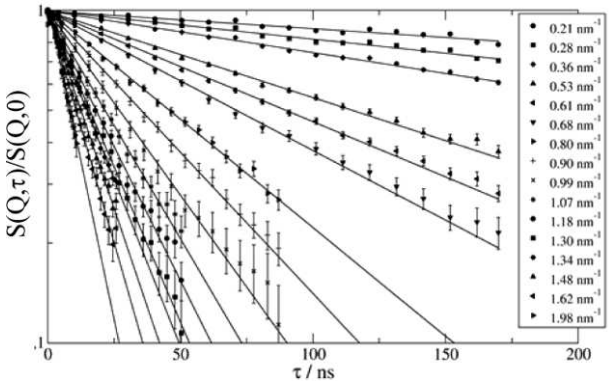

Figure 7. Neutron spin echo results on a 1% ADH resolution at 5°C without cofactor for various momentum transfers.

for solution structures. Let us commence with the inset: here for different concentrations the low Q data are presented and there the increasing influence of the structure factor on the SANS data is visible. In the main figure the low concentration data are presented over the full Q range and are compared with different structural models. The solid line reflects the crystal structure which appears to be in perfect agreement with the solution data. Testing the sensitivity of the approach we compare with a situation, where we bring the two dimers in a planar configuration into close contact. The results are presented by the dashed line which in particular at high momentum transfers leads to an underestimation of the scattering data. Furthermore, using the programme DAMMIN [19] which builds SANS scattering curves from an arrangement of small mesoscopic spheres also allows a perfect fit of the experimental data (result superimposes with the crystal results) and confirms the crystal-based perpendicular arrangement of the two dimers. Thus, we conclude that as in the crystal, the ADH tetramer in solution is present in a crossed dimer configuration.

The overall molecular diffusion was measured by dynamic light scattering and was found to be independent of concentration. The translational diffusion coefficient amounts to $D_{\mathrm{DLS}} = 23.5 \pm 2\ \mu\mathrm{m}^2/\mathrm{s}$ at 5°C corresponding to a hydrodynamic radius of $R_{\mathrm{H}} \cong 4.5$ nm.

Neutron spin echo data were measured at different concentrations with and without the cofactor NAD. Figure 7 displays NSE results in a logarithmic fashion for a large number of different momentum transfers Q. In each case single exponential fits are included showing that the measured structure factor may be described in terms of a single exponential decay.

Comparing the covered Q range with the SANS data, one realizes that both the range of the structure factor, where intermolecular interactions are important as well as the regime of internal structure are covered. Considering that all data may be described in terms of a single exponential decay, we approximate the spectra in terms of a first cumulant expansion taking the initial slope $\Gamma(Q)$ of the structure factor as a measure for the dynamics. This gives an effective diffusion coefficient

$$D_{\mathrm{eff}}(Q) = \frac{\Gamma(Q)}{Q^2}. \tag{5}$$

Figure 8 presents these effective diffusion coefficients as a function of Q for different concentrations with and without NAD. The line at low Q indicates the level of the light scattering result. The data were corrected for the influence of the structure factor and for hydrodynamic interactions [13] (D^0_{eff}). The experimental data show a strong Q modulation exhibiting a maximum around $Q = 1\ \mathrm{nm}^{-1}$. We also see that beyond the statistical error in the low Q flank the relaxation without NAD is somewhat faster than that including the cofactor. Thus, in the dynamics of ADH on the scale of the molecule itself we observe significant contributions beyond translational diffusion. This observed higher Q structure is entirely determined by intra-aggregate effects.

The prime reasons for a Q-dependent structure in $D_{\mathrm{eff}}(Q)$ are rotational motions of the molecule. In a first cumulant approximation the effective diffusion coefficient of a rigid body undergoing translational and rotational diffusions has the following form [20]:

$$D_{\mathrm{eff}}(Q) = \frac{k_{\mathrm{B}}T}{Q^2} \frac{\sum_{jK} \left\langle b_j \mathrm{e}^{i\underline{Q}\underline{r}_j} \begin{pmatrix} \underline{Q} \\ \underline{Q} \times \underline{r}_j \end{pmatrix} \bar{H} \begin{pmatrix} \underline{Q} \\ \underline{Q} \times \underline{r}_K \end{pmatrix} b_K \mathrm{e}^{-i\underline{Q}\underline{r}_K} \right\rangle}{\sum_{jK} \langle b_j \mathrm{e}^{i\underline{Q}\underline{r}_j} b_K \mathrm{e}^{-i\underline{Q}\underline{r}_K} \rangle}. \tag{6}$$

Here $\underline{r}_i$ and $\underline{r}_K$ are the atomic coordinates, b_i and b_K the corresponding neutron scattering lengths and $\bar{H}$ the mobility tensor. The sums run over all atoms of the molecule or molecular aggregate and the pointed brackets indicate an ensemble average. The denominator resembles the aggregate form factor. The mobility matrix $\bar{H}$ is a 6×6 tensor involving translational and rotational parts including a translational rotational coupling. Further evaluation of eq. (6) was performed using the program HYDROPRO developed by Garcia de la Torre and coworkers [21]. The rotational averaging was performed numerically with small step sizes. The

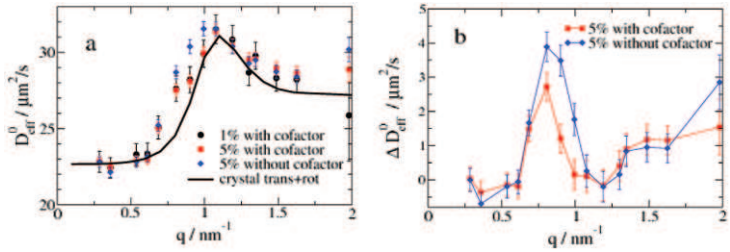

Figure 8. (**a**) Comparison of the corrected effective diffusion coefficient with the prediction for rigid body motion. (**b**) Difference between the rigid body dynamics and the observed effective diffusion coefficients.

calculations with HYDROPRO need as an input the crystallographic coordinates of all atoms.

In figure 8a all data sets for $D_{\text{eff}}(Q)$ at 1%, 5%, with and without NAD are compared. Thereby $D_{\text{eff}}(Q)$ was rescaled with the structure factor. We realize that after rescaling the diffusion coefficient in the region above $Q = 0.6$ nm^{-1} all data sets are consistent. We note that the data at 5% solution are of significantly higher statistical accuracy underlining the deviation from pure rotational motion even more strongly. Furthermore, the sample with cofactor compared to that without NAD exhibits a somewhat slower dynamics in the low Q flank of the peak in $D_{\text{eff}}(Q)$. Given the overall consistency of the data points and the size of the error bars this difference in the dynamic response appears to be significant and indicates some influence of the binding of NAD on the overall molecular dynamics. Using the crystal-based crossed dimer model we obtain the solid curve in figure 8a describing the overall shape of $D_{\text{eff}}(Q)$ quite well but misses the proper low and high Q-flanks. These differences between the rotational diffusion expectation for a rigid aggregate and the experimental data are displayed in figure 8b. We note that at Q values below the peak of the rigid body rotational diffusion coefficient significantly faster effective diffusion takes place. This result indicates the presence of internal motion within the molecule which must involve mainly those atoms which are placed in the outer regions of the tetramer emphasizing more strongly the larger distances within the molecule and therefore giving rise to extra dynamics at low Q.

At present we evaluate these differences in terms of a normal mode analysis indicating that they result from fluctuations of the more flexible outer part of the tetramer [13]. In such a picture the differences in the low Q flank of the data from the aggregate with and without the cofactor seem to indicate a significant difference of the configurational stiffness of the protein depending on the presence of cofactor [22].

We have presented some representative results from neutron spin echo spectroscopy on the dynamics of macromolecules. In the case of linear chains we have shown that the large-scale dynamics may be well understood in terms of confinements giving rise to tube constraints as stated by the reptation model. As the leading reptation limiting processes the NSE data have quantitatively confirmed contour length fluctuations destroying the tube confinements from the ends. Furthermore, we have presented some first experimental data on the component

fluctuations of a tetrameric aggregate formed by alcohol dehydrogenase. It became possible to directly measure the Q-dependent effective diffusion coefficient which bears information on the internal dynamics of the protein complex.

References

[1] For a recent review, see, *Advances in polymer science* edited by D Richter, M Monkenbusch, A Arbe and J Colmenero (Springer, Berlin, Heidelberg, 2005) Vol. 174
[2] M Doi and S F Edwards, *J. Chem. Soc., Faraday Trans.* **274**, 1789 (1978); **274**, 1802 (1978)
[3] P G de Gennes, *J. Chem. Phys.* **55**, 572 (1971)
[4] Z Bu, R Biehl, M Monkenbusch, D Richter and J E Callaway, *Proc. Natl. Acad. Sci. (USA)* **102**, 17646 (2005)
[5] Neutron Spin Echo, *Lecture Notes in Physics* edited F Mezei (Springer, Berlin, Heidelberg, 1980) Vol. 128
[6] A Wischnewski, M Monkenbusch, L Willner, D Richter, B Farago and G Kali, *Phys. Rev. Lett.* **90**, 058302 (2003)
[7] H Montes, M Monkenbusch, L Willner, S Rathgeber, L J Fetters and D Richter, *J. Chem. Phys.* **110**, 10188 (1999)
[8] P Schleger, B Farago, C Lartigue, A Kollmar and D Richter, *Phys. Rev. Lett.* **81**, 124 (1998)
[9] T C B McLeish, *Adv. Phys.* **51**, 1 (2002)
[10] A Wischnewski, M Monkenbusch, L Willner, D Richter, A E Likhtmann, T C B McLeish and B Farago, *Phys. Rev. Lett.* **88**, 058301 (2002)
[11] M Zamponi, M Monkenbusch, L Willner, A Wischnewski, B Farago and D Richter, *Europhys. Lett.* **72**, 1039 (2005)
[12] M Zamponi, A Wischnewski, M Monkenbusch, L Willner, D Richter, A E Likhtmann, G Kali and B Farago, *Phys. Rev. Lett.* **96**, 238302 (2006)
[13] R Biehl, M Monkenbusch, D Richter, B Hoffmann and R Merkel, to be published
[14] M Doi and S F Edwards, *The theory of polymer dynamics* (Clarendon, Oxford, 1986)
[15] P G de Gennes, *J. Phys. (Paris)* **42**, 735 (1981)
[16] A E Likhtmann and T C B McLeish, *Macromolecules* **35**, 6332 (2002)
[17] N Clark and T C B McLeish, *Macromolecules* **26**, 5264 (1993)
[18] F Schotte, M Lim, T A Jackson, A V Smirnov, J Soman, J S Olson, G N Philips Jr, M Wulff and P A Aninfrud, *Science* **300**, 1944 (2003)
[19] D I Svergun, *Biophys. J.* **76**, 2879 (1999)
[20] N Brown, Dynamic light scattering, in: *Monographs on the physics and chemistry of materials* (Oxford Science Publications, Oxford, 1993) Vol. 49
[21] J Garcia de la Torre, M L Huertas and B Carrasco, *Biophys. J.* **78**, 719 (2000)
[22] R Biehl, B Hoffmann, M Monkenbusch, P Falus, S Prévost, R Merkel and D Richter, *Phys. Rev. Lett.* (2008) in print